The Generation of 400-MW RF Pulses at X-Band Using Resonant Delay Lines

Sami G. Tantawi, *Member, IEEE,* Roderick J. Loewen, Christopher D. Nantista, and Arnold E. Vlieks

***Abstract*—In this paper, we present theory and experimental data for a resonant-delay-line pulse-compression system. The system is fed by two high-power klystrons at X-band. The peak output power is four times the input power. The system produces flat-top output pulses. It uses evacuated room-temperature copper delay lines as a means of storing energy. These lines achieved a quality factor greater than 4.3×10^5, with total losses due to external components measured at 4%. We compare theory with experimental results. The system produced 150-ns pulses at power levels around 470 MW.**

I. Introduction

RADIO-FREQUENCY pulse compression using resonant delay lines is proposed as a method for achieving the high-power flat RF pulse required to drive the next linear collider (NLC) [1], [2]. In order to achieve pulse compression, energy from an incoming RF pulse is stored in high-Q resonant delay lines. While charging, energy that leaks out of the delay lines is, to a great extent, canceled by the reflected incident RF. To discharge the lines, the phase of the incoming pulse is reversed so that the reflected signal from the inputs to the lines adds constructively with the emitted field from the stored energy in the lines for the duration of one round-trip time of RF in the line.

The system suffers from two types of losses that reduce its efficiency: intrinsic losses and finite conductivity losses. By design, some of the input energy is immediately reflected at the delay-line entrance during the charging phase. Additionally, after the phase reversal, the energy inside the lines is not discharged completely at the desired compressed pulse time period. Unfortunately, the coupling coefficient to the line that maximizes the energy storage makes the energy discharge from the line far from optimum. The system is designed for an optimum coupling coefficients at a specific compression ratio to maximize the output power [3]. During the period of time the RF energy spends inside the storage line, part of it is lost simply due to the finite quality factor of the lines. Similar losses occur from the finite conductivity of the components used to manipulate the input and output signals.

We describe the experimental procedures and the measurements performed on the high-power X-band prototype built at the Stanford Linear Accelerator Center (SLAC), Stanford University, Stanford, CA.

Manuscript received March 26, 1999; revised July 12, 1999. This work was supported by the Department of Energy under Contract DE-AC03-76SF00515.

S. G. Tantawi is with the Stanford Linear Accelerator Center, Stanford University, Stanford, CA 94309 USA, and is also with the Communications and Electronics Department, Cairo University, Giza, Egypt.

R. J. Loewen, C. D. Nantista, and A. E. Vlieks are with the Stanford Linear Accelerator Center, Stanford University, Stanford, CA 94309 USA.

Publisher Item Identifier S 0018-9480(99)08453-7.

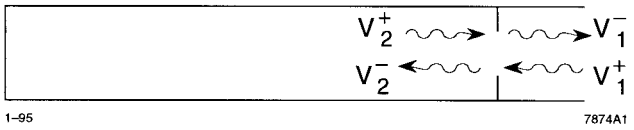

Fig. 1. Resonant delay line.

II. Theory

A. Resonant Delay-Line Pulse-Compression Theory

Consider a waveguide delay line terminated by a short circuit and coupled at its input with a coupling iris, as shown in Fig. 1. The lossless scattering matrix representing the iris is unitary. At a certain reference plane, the matrix takes the following form:

$$\underline{\underline{S}} = \begin{pmatrix} -R_0 & -j(1-R_0^2)^{1/2} \\ -j(1-R_0^2)^{1/2} & -R_0 \end{pmatrix}. \tag{1}$$

In writing (1), we assumed a symmetrical structure for the iris two port network. The forward and reflected fields around the iris are related as follows:

$$V_1^- = -R_0 V_1^+ - j(1-R_0^2)^{1/2} V_2^+ \tag{2}$$

$$V_2^- = -j(1-R_0^2)^{1/2} V_1^+ - R_0 V_2^+. \tag{3}$$

With the exception of some phase change, the incoming signal V_2^+ at time instant t is the same as the outgoing signal V_2^- at time instant $t-\tau$, where τ is obviously the round-trip delay through the line, i.e.,

$$V_2^+(t) = V_2^-(t-\tau)e^{-j2\beta l} \tag{4}$$

where β is the wave propagation constant within the delay line and l is the length of the line. Substituting from (4) into (3), we get

$$V_2^-(t) = -j(1-R_0^2)^{1/2} V_1^+(t) - R_0 V_2^-(t-\tau)e^{-j2\beta l}. \tag{5}$$

During the charging phase, we assume a constant input, i.e., $V_1^+(t) = V_{\mathbf{in}}$, which equals a constant value. We also assume that all the voltages are equal to zero at time $t < 0$. Hence, substituting the solution of the difference equation (5) into (4) leads us to write

$$V_2^+(i) = -j\,\frac{1-\left(-R_0 e^{-j2\beta l}\right)^i}{1+R_0 e^{-j2\beta l}}\,(1-R_0^2)^{1/2} e^{-j2\beta l} V_{\mathbf{in}}. \tag{6}$$

In (6), $V_2^+(i)$ means the incoming wave in the time interval $i\tau \le t < (i+1)\tau$ and $i \ge 0$. Substituting from (6) into (2), we get

$$V_1^-(i) = -V_{\text{in}}\left[R_0 + (1-R_0^2)\,\frac{1-\left(-R_0e^{-j2\beta l}\right)^i}{1+R_0e^{-j2\beta l}}\,e^{-j2\beta l}\right]. \tag{7}$$

If the delay line has small losses (β has a small imaginary part), at resonance the term

$$e^{-j2\beta l} = -p \tag{8}$$

where p is a positive real number close to one. Equation (7) becomes

$$V_1^-(i) = -V_{\text{in}}\left[R_0 - (1-R_0^2)\,\frac{1-(R_0p)^i}{1-R_0p}\,p\right]. \tag{9}$$

After the energy has been stored in the line, one may dump part of the energy in a time interval τ by flipping the phase of the incoming signal just after a time interval $(n-1)\tau$, i.e.,

$$V_1^+(t) = \begin{cases} V_{\text{in}}, & 0 \le t < (n-1)\tau \\ -V_{\text{in}}, & (n-1)\tau \le t < n\tau \\ 0, & \text{otherwise.} \end{cases} \tag{10}$$

The output pulse level during the time interval $(n-1)\tau \le t < n\tau$ can be calculated from (2) with the aid of (6). The result is

$$V_{\text{out}} = V_1^-(n-1) = V_{\text{in}}\left[R_0 + (1-R_0^2)\,\frac{1-(R_0p)^{n-1}}{1-R_0p}\,p\right]. \tag{11}$$

Indeed, this is the essence of the pulse-compression system.

The maximum power gain of the system is limited. Using (11), the power gain as $n \to \infty$ is

$$\left(\frac{V_{\text{out}}}{V_{\text{in}}}\right)^2\Bigg|_{n\to\infty} = \left[R_0 + (1-R_0^2)\,\frac{p}{1-R_0p}\right]^2 \tag{12}$$

which has a maximum value of

$$\text{Maximum Power Gain} = \frac{17}{p^2} - 8 - \frac{12\sqrt{2(1-p^2)}}{p^2} \tag{13}$$

at

$$R_0 = \frac{1}{p} - \frac{\sqrt{8(1-p^2)}}{4p}. \tag{14}$$

Clearly, the maximum power gain is limited to nine as $p \to 1$ Furthermore, this maximum is greatly affected by the losses in the delay line; e.g., the gain is limited to 7.46 if the line has a 1% round-trip power losses.

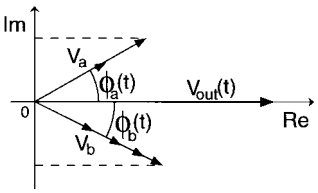

Fig. 2. Phasor diagram showing the voltage during the compressed pulse as composed of contributions from six time bins, phase modulated so as to form two phasors rotating in time. Cancellation of the imaginary parts is maintained while the sum or the real parts yields a constant-phase output voltage of changing amplitude.

B. Pulse Shaping

The primary reason for developing this RF pulse compressor is to drive high-gradient electron accelerator structures for use in future linear colliders. When trains of many bunches are accelerated on one RF pulse in a traveling-wave accelerating structure, the leading bunches tend to diminish the energy density in the structure, causing the trailing bunches to receive less acceleration. This energy spread problem can be solved by preloading the structure with a ramped RF profile [4]. Hence, the pulse compressor needs to have the ability to shape the RF pulse. We can obtain such a ramp followed by a flat-top from our pulse-compression system by varying the input signal phase within each τ time bin while keeping the amplitude fixed.

The effect of multiple reflections in the delay lines is made explicit if (11) is recast as

$$V_{\text{out}} = V_{\text{in}}\left[R_0 + (1-R_0^2)p\sum_{m=1}^{n-1}(R_0p)^{m-1}\right]. \tag{15}$$

If we relax the assumption that V_{in} is constant, this must be written

$$V_{\text{out}} = R_0V_{\text{in}}(n) + (1-R_0^2)p\sum_{m=1}^{n-1}(R_0p)^{n-m-1}V_{\text{in}}(m). \tag{16}$$

Let each of the n time bins be given one of two phase profiles so that their contributions to the compressed pulse form two phasors

$$\tilde{V}_a(t) = V_ae^{j\phi_a(t)} \quad \text{and} \quad \tilde{V}_b(t) = V_be^{j\phi_b(t)} \tag{17}$$

with

$$V_a = R_0 + (1-R_0^2)p\sum_{m\in A}(R_0p)^{n-m-1} \tag{18}$$

$$V_b = (1-R_0^2)p\sum_{m\in B}(R_0p)^{n-m-1}. \tag{19}$$

Here, A and B indicate the subsets of time-bin numbers assigned to either phasor. These subsets do not include the nth time bin, which gives the first term in V_a. These phasors can be swept in phase in such a way that their imaginary parts always cancel and their real parts yield a ramped output amplitude (see Fig. 2). The closer in amplitude the phasors can be made by judicious grouping, the greater the range over

which the amplitude can be swept since the resultant amplitude can be varied between e

$$V_{\min} = \sqrt{|V_a^2 - V_b^2|} \tag{20}$$

and

$$V_{\max} = V_a + V_b. \tag{21}$$

Beam loading compensation for a constant-gradient structure requires a linear ramp [4]. We set

$$\begin{aligned} \operatorname{Re} V_{\text{out}}(t_n') &= V_a \cos \phi_a(t_n') + V_b \cos \phi_b(t_n') \\ &= V_0 + \Delta V \frac{t_n'}{\Delta t}, \qquad 0 \le t_n' \le \Delta t \end{aligned} \tag{22}$$

$$\begin{aligned} \operatorname{Im} V_{\text{out}}(t_n') &= V_a \sin \phi_a(t_n') + V_b \sin \phi_b(t_n') \\ &= 0 \end{aligned} \tag{23}$$

where $t_n' = t - (n-1)\tau$, $V_{\min} \le V_0 \le V_{\max}$, and $\Delta V = V_{\max} - V_0$. $\Delta t < \tau$ is the desired ramp duration, i.e., the fill time minus the transit time of the accelerator structure. The solution is

$$\phi_a(t) = \begin{cases} \cos^{-1}\left[\dfrac{1}{2V_a}\left(V_0 + \Delta V \dfrac{t}{\Delta t} - \dfrac{V_b^2 - V_a^2}{V_0 + \Delta V t/\Delta t}\right)\right], \\ \qquad 0 \le t < \Delta t \\ 0, \qquad \Delta t \le t \le \tau \end{cases} \tag{24}$$

$$\phi_b(t) = \sin^{-1}\left(-\frac{V_a}{V_b} \sin \phi_a(t)\right). \tag{25}$$

Fig. 3 illustrates this method of pulse shaping. Note that the pulse compression phase flip before the last time bin is required, with the above phase pattern superimposed.

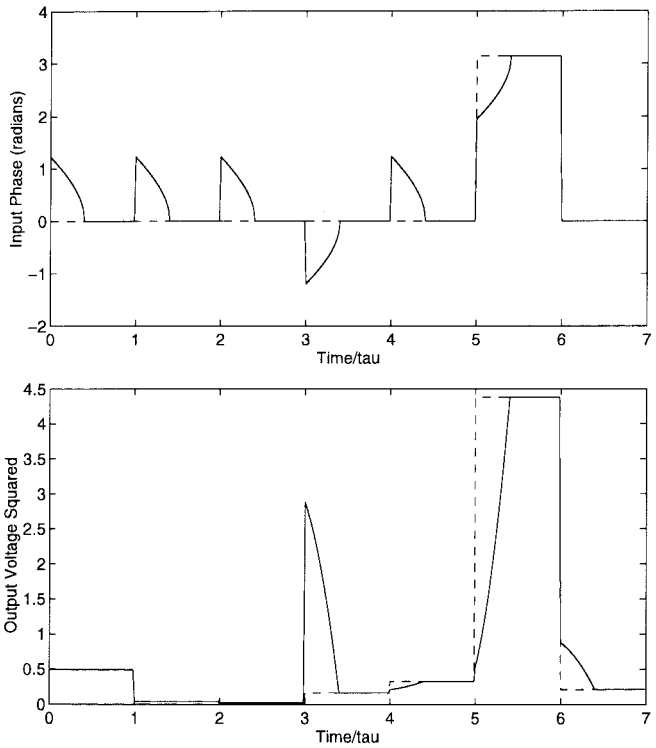

Fig. 3. Pulse shaping with resonant-delay-line pulse compression. The beginning portion of each time bin is phase modulated with one of two functions (in addition to the phase flip). The compressed output pulse acquires a ramp. The missing energy in this example is largely moved to the fourth time bin of the output waveform. Dashed lines show the corresponding waveforms without pulse shaping.

III. System Implementation

To separate the input signal from the reflected signal, one might use two delay lines fed by a 3-dB hybrid, as shown in Fig. 4. The reflected signal from both lines can be made to add at the forth port of the hybrid. Fig. 4. shows the pulse-compression system. For delay lines, it uses two 22.48-m-long cylindrical copper waveguides, each is 12.065 cm in diameter and operating in the TE_{01} mode. In theory, these over-moded delay lines can form a storage cavity with a quality factor $Q > 1 \times 10^6$. A shorting plate, whose axial position is controllable to within ± 4 μm by a stepper motor, terminates each of the delay lines. The input of the line is tapered down to a 4.737-cm diameter waveguide at which the TE_{02} mode is cut off; hence, the circular irises that determine the coupling to the lines do not excite higher order modes provided that they are perfectly concentric with the waveguide axis.

A compact low-loss mode converter excites the TE_{01} mode just before each iris. These mode transducers, known as wraparound mode converters, were developed specifically for this application. The mode converters are connected to two uncoupled arms of a high-power over-moded planar 3-dB hybrid. This hybrid is also designed specially for this application so that it can handle the super-high power produced by this system. The distance from the irises to the center of the hybrid has been adjusted to within ± 13 μm to minimize reflections to the input port. The iris reflection coefficient is optimized for a compression ratio of eight.

The system is designed to operate under vacuum. All the components are designed to handle the peak fields required by the high-power operating conditions of the system. In what follows, we will describe the design of each component.

A. The Wraparound Mode Converter

The delay lines are fed by a mode transducer that converts the RF signal from the TE_{10} mode in rectangular guide to the low-loss TE_{01} mode in circular guide. A schematic diagram of this mode transducer is shown in Fig. 5(a) and (b), and the physical model is shown in Fig. 5(c). The converter is basically composed from a circular waveguide fed from the side by a number of rectangular waveguides. The orientation of these rectangular guides is such that their transverse magnetic field is parallel to the circular waveguide axis. Hence, only TE modes are excited in the circular guide. If the signals from all the rectangular guides are equal in phase and amplitude, the only modes that can get excited in the circular guide are TE_{mn} and TE_{0n}, where m is the number of rectangular waveguides feeding the circular guide. The cut off frequency of the TE_{01} mode is greater than the cutoff frequency of the TE_{31} mode but smaller than the cutoff frequency of the TE_{41} mode or

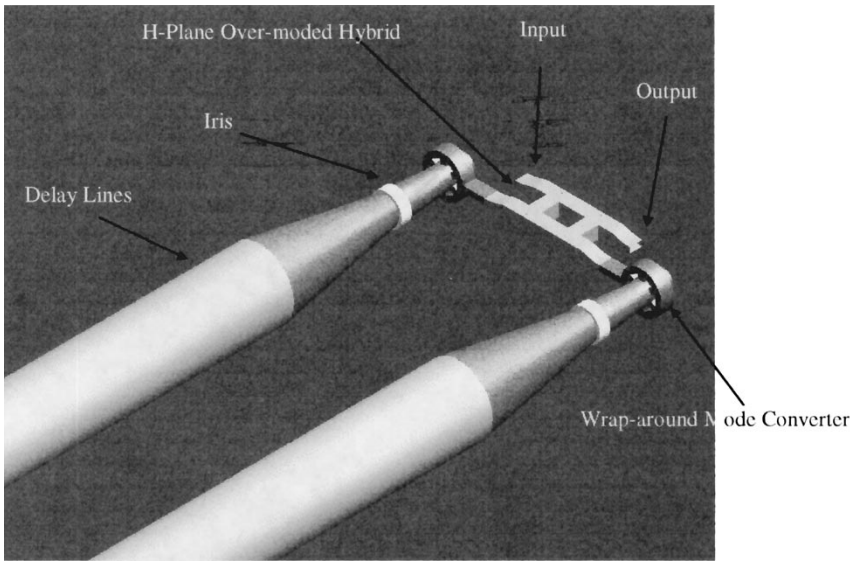

Fig. 4. Resonant delay-line pulse-compression system.

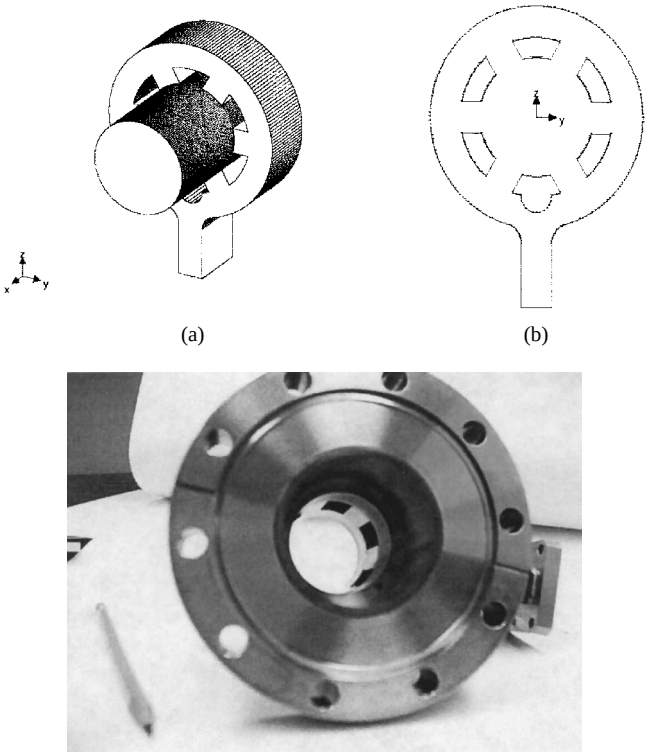

Fig. 5. Wraparound mode converter. The physical model shown does not have the back-wall shorting plate, this is done for illustration purposes only.

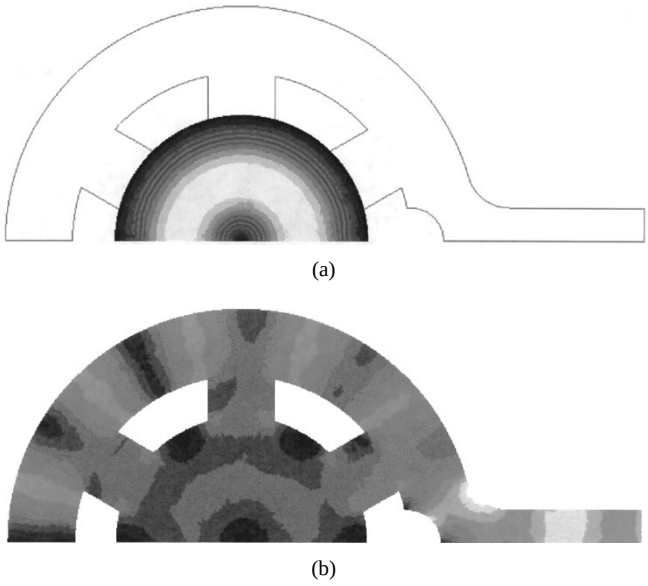

Fig. 6. HFSS simulation results for the wraparound mode converter. The different shades represent the magnitude of the electrical field. (a) A cut plane through the slots. (b) A cut plane in the circular guide 2.5 cm away from the slots.

any TE_{m1} mode, where $m \geq 4$. Therefore, if $m \geq 4$, i.e., the number of rectangular guides is greater than or equal to four. The circular guide diameter can be chosen such that TE_{01} is the only propagating mode that can get excited. In this converter, the number of rectangular waveguides is six.

To get an equal excitation through the internal coupling rectangular guides, a single common rectangular guide feeds them. This guide is wrapped around the device. Due to the geometrical and excitation symmetry around the ZX-plane, one-half of the device needs to be considered, as shown in Fig. 6(a). From a circuit point-of-view, the curved rectangular guide should feed the rectangular guides [as shown in Fig. 6(a)] at an interval of $n\lambda_g$, where λ_g is the wavelength curve guide and n is an integer. In this case, $n = 1$. The short circuit at the end of the curved guide, produced by the symmetry plane, should be located $\lambda_g/4$ away from the last waveguide feed. A bulge splits the power around the symmetry plane at the entrance of the rectangular guide, as shown in Fig. 6(a).

The final design dimensions were carried out using HFSS.[1] The field in a cross section of the circular guide that contains

[1] "HP high-frequency structure simulator," HP EEsof, Hewlett-Packard Company, Santa Rosa, CA.

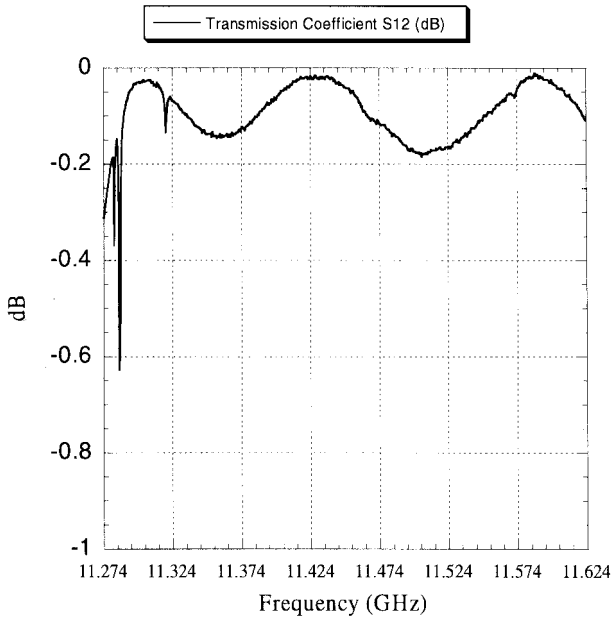

Fig. 7. Transmission coefficient for two wraparound mode converters back to back. The device is optimized at 11.424 GHz.

the feeding rectangular guides is shown in Fig. 6(a). Away from the slot perturbation, the field in the circular guide is shown in Fig. 6(b).

The device, as described, is basically a three-port device: one rectangular input and two circular outputs. One of the design criterions was to achieve the following scattering matrix for the three-port device:

$$S = \begin{pmatrix} -1/3 & 2j/3 & 2j/3 \\ 2j/3 & 1/3 & -2/3 \\ 2j/3 & -2/3 & 1/3 \end{pmatrix}. \tag{26}$$

With this scattering matrix, shorting one of the circular ports would achieve a perfect transmission between the remaining two ports. We could approach this matrix, but not perfectly. The remaining small mismatch after shorting one of the circular ports was a reflection coefficient of 0.21. The device was matched using an iris in the circular waveguide. The matching was done in circular guide to avoid enhancing the field in the rectangular guide. Fig. 7 shows transmission measurements of two mode converters connected back to back from their circular ports.

B. The 3-dB Hybrid

We have developed a novel design for a waveguide hybrid, or 3-dB directional coupler, capable of handling hundreds of megawatts of peak RF power at X-band (11.424 GHz). It consists of four rectangular waveguide ports connected through four H-plane T-junctions, yielding a two-rung ladder geometry, as shown in Fig. 8. The H-plane symmetry allows the use of over-moded rectangular waveguide in which the height has been increased to reduce field amplitudes without affecting the scattering matrix. Small apertures, slots, and field-enhancing e-bends are avoided to reduce the risk of RF breakdown. The device is a quadrature hybrid (i.e., the coupled

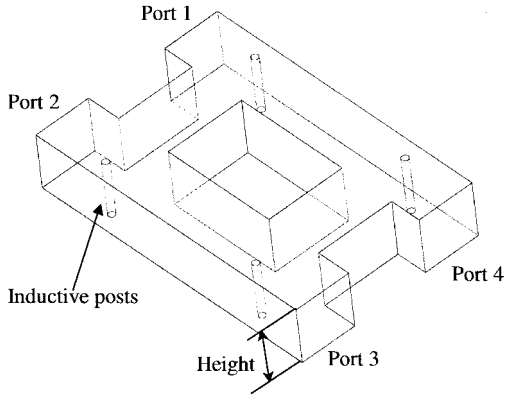

Fig. 8. Schematic diagram of the over-moded H-plane hybrid.

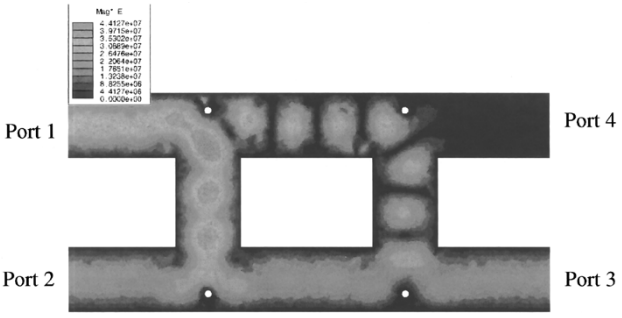

Fig. 9. HFSS simulation results of the H-plane hybrid. The different shades represents the magnitude of the electrical field. Port 1 is being excited. Note that Port 1 is completely isolated from Port 2.

port fields are 90° out of phase), and directly opposite ports are isolated.

This hybrid is a realization in rectangular waveguide of Dicke's synthesis of a biplanar Magic-T [5] or of a modified microstrip branch-line hybrid. In a transmission line, this requires the distances between all adjacent junctions to be ($n/2$ plus) one quarter-wavelength and the two connecting lines to have a characteristic admittance that is $\sqrt{2}$ times that of the main guides. In waveguide, the two-dimensional geometry necessitates matching elements in the T-junctions to adjust the complex impedances.

A mode-matching code was used to determine the radius and placement of posts that would yield the desired three-port junction scattering matrix from which the hybrid ring circuit could then be constructed. The fields were expanded in cylindrical harmonics about the post in the junction region and in normal modes in the rectangular ports. The synthesized hybrid design was then checked with HFSS. The resultant fields are shown in Fig. 9. Note that port 4 is completely isolated from port 1. The cold test measurements of the hybrid model are shown in Fig. 10. The port numbers are those described in Fig. 8.

IV. Cold Test Measurements

All measurements were performed using an HP8510C network analyzer with the results examined in the time domain using a PC. The frequency-domain measurements were transferred to the PC via a general-purpose I/O bus (GPIB) link and

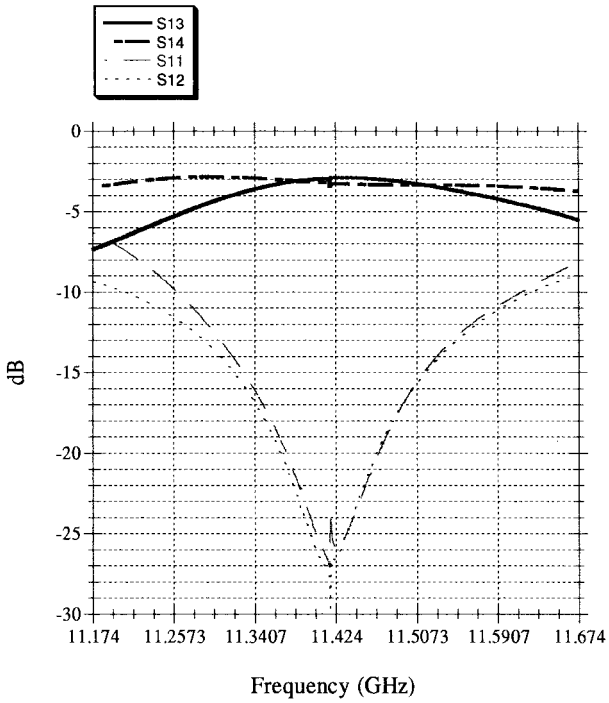

Fig. 10. Cold test measurements of the H-plane hybrid. The parameters of the hybrid were optimized at 11.424 GHz.

multiplied by the fast Fourier transform (FFT) of a maximally flat pulse modulating an 11.424-GHz signal. If we define the compressed pulsewidth as τ (equal to the round-trip time of the RF through the delay line), the input pulsewidth should be of the form $n\tau$, where n is an integer equal to the compression ratio. For a given compression ratio, the phase of the input pulse should be reversed 180° at the time $\tau(n-1)$. In our case, the value of τ is fixed at 150 ns. The test pulse has the following form:

$$V_{\text{in}}(t) = \frac{1}{\sqrt{1+\left(\frac{2t}{\tau n}\right)^{2l}}} - \frac{2}{\sqrt{1+\left(2\frac{\left(t-\frac{\tau(n-1)}{2}\right)}{\tau}\right)^{2k}}} \tag{27}$$

where l controls the pulse rise time and k controls the phase reversal rise time. The time-domain output is produced by taking the inverse FFT (IFFT) of this frequency-domain product. Note that once we obtain the frequency characteristics of the system from the network analyzer, we can calculate the time-domain response for any arbitrary input pulse.

In order to determine the RF losses of the 3-dB hybrid/mode transducer assembly, the circular ends of the mode transducers were shorted and the round-trip transmission was measured to be greater than 97%. The reflections from the input and output ports was also measured to be less than -26 dB. The delay lines were then attached and brought into resonance at 11.424 GHz with the adjustable shorts. Fig. 11 shows the measured frequency response of the system. Fig. 12 shows the response of the system to a pulse described by (27) for a pulsewidth of 1.2 μs (a compression ratio of 8). Using (11),

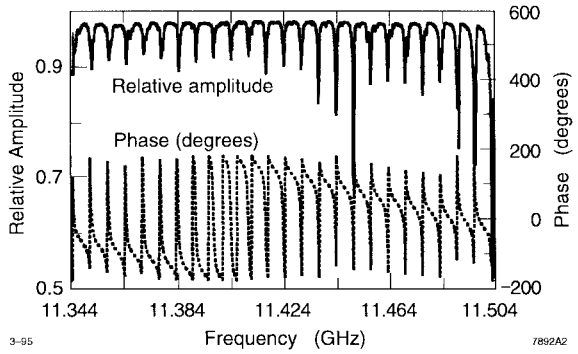

Fig. 11. Pulse compressor measured frequency response in magnitude and phase.

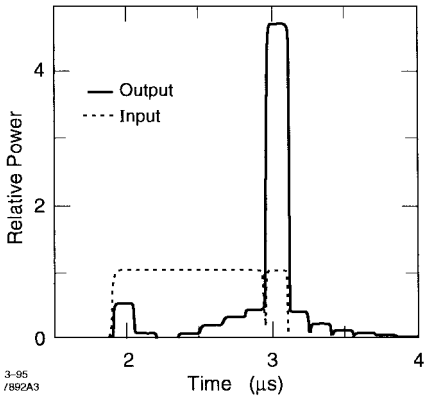

Fig. 12. Pulse compressor output for a compression ratio of eight: input pulsewidth of 1.2 μs and output pulsewidth of 0.15 μs.

the power gain of the compressed pulse can be written as

$$\text{Power Gain} = \left[R_0 + (1-R_0^2)\frac{1-(R_0p)^{n-1}}{1-R_0p}\,p\right]^2(1-x) \tag{28}$$

where R_0 is the iris reflection coefficient, x is the power losses due to external components (the Magic-T/mode transducer assembly), and $(1-p^2)$ is the round-trip loss in the transmission lines. This last quantity is related to the intrinsic quality factor of the line [6] by

$$Q = \frac{\pi f_0 t_d}{-\ln(p)}. \tag{29}$$

The power gain was measured for a series of compression ratios. A least-squares fitting of these measurements to (28) with the fit parameters R_0, x, and $(1-p^2)$ is shown in Fig. 13. The round-trip losses was found to be 2.45%, indicating an intrinsic Q for the lines of 4.3×10^5. The external losses are 4%, and the iris reflection coefficient is 0.74. The iris was designed using a mode-matching code to have a reflection coefficient of 0.73, the optimum value for a compression ratio of eight.

V. High-Power Setup and Results

The experimental setup consisted of an RF source, a resonant delay-line pulse compressor, and a high-power load

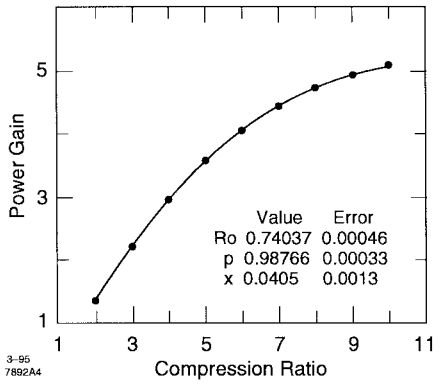

Fig. 13. The points are measured power gains for different compression ratios. The curve represents the least squares fit for the parameters in (28) with values as shown in the table.

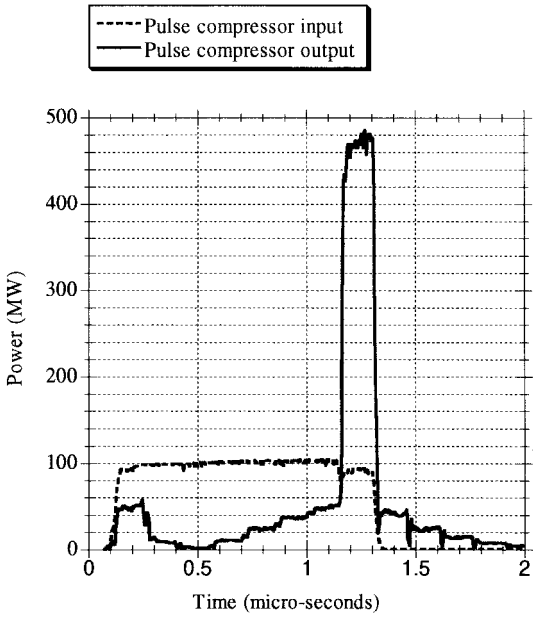

Fig. 14. High-power input and output signals. The output pulse has a power level in excess to 470 MW.

assembly. The combined power of two 50-MW klystrons [7], [8], operating at 11.424 GHz, supplies the RF power to the pulse compressor. Under the highest power operating conditions, these klystrons were operated at approximately 10%–15% above their nominal power levels. The pulsewidth of each klystron was 1.2 μs running at a repetition rate of 60 Hz. The input power to each klystron originates at a common signal generator. The low-level signal is first split and then sent to a pair of 180° fast phase shifters (rise time of shift $<$10 ns). A fast rise-time command pulse initiates the phase inversion of the RF signal. The purpose of these phase shifters is to permit the pulse compressor to deliver the high-power pulse at the appropriate time bin. (See Section II.)

The output signal from each phase shifter is first amplified and then sent to 2.5-kW TWT amplifiers through WR90 waveguides. A variable attenuator in this line permits saturation of each TWT. Finally, the TWT provides the input drive power to each klystron through a variable attenuator.

Since the relative phasing of the two klystrons at the four-port combiner (Magic-T) determines how the power level is divided between the output ports, a phase shifter is employed in the input arm of one of the klystrons. This phase shifter is adjusted to direct all of the klystrons' power into the input arm of the pulse compressor.

The output power from the pulse compressor was delivered to a pair of high-power load assemblies. The power was first split by an H-plane hybrid so that half the power was supplied to each assembly. One assembly consisted of four choked stainless-steel "dry" loads [9] arranged in parallel. (A Magic-T first splits the incoming power and then two additional Magic-T's divide each of the split power levels again.) The second assembly consisted of two additional "dry" loads also arranged in parallel. These loads were similar to those in the first assembly, except they were designed to handle twice the average power.

Fig. 14 shows the input and output pulse shapes of the compressor. The output power level is about 470 MW, the maximum power achieved by the system. The power was limited by the available power from the combined klystrons. This power level was achieved after 60 h of processing.

VI. Conclusion

We presented an implementation of a super-high-power resonant-delay-line pulse-compression system. The output of the system agrees well with theory. The over-moded components and mode converters have proven to be capable of handling these levels of RF power at X-band.

Acknowledgment

The authors are grateful for the many useful dissections with Prof. P. Wilson, Prof. R. Ruth, Prof. N. Kroll, and D. Z. Farkas.

References

[1] R. D. Ruth *et al.*, "The next linear collider test accelerator," in *Proc. IEEE Particle Accelerator Conf.*, Washington DC, May 1993, pp. 543–545.

[2] P. B. Wilson, Z. D. Farkas, and R. D. Ruth, "SLED II: A new method of RF pulse compression," in *Linear Accelerator Conf.*, Albuquerque, NM, Sept. 1990, SLAC-PUB-5330.

[3] S. G. Tantawi *et al.*, "Active radio frequency pulse compression using switched resonant delay lines," in *Nuclear Instruments & Methods in Physic Research, Section A (Accelerators, Spectrometers, Detectors and Associated Equipment).* New York: Elsevier, 1996, pp. 297–302.

[4] "Next linear collider test accelerator conceptual design report," SLAC, Stanford Univ., Stanford, CA, Rep. 411, Aug. 1993.

[5] C. G. Montgomery, R. H. Dicke, and E. M. Purcell, Eds., *Principles of Microwave Circuits* (MIT Radiation Lab. Series 8). Boston, MA; Tech. Lithographers, 1963, p. 451.

[6] C. D. Nantista, "Radio-frequency pulse compression for linear accelerators," SLAC, Stanford Univ., Stanford, CA, Rep. 96-455, p. 54, Jan. 1995.

[7] G. Caryotakis *et al.*, "The X-band klystron program at SLAC," in *Proc. 3rd Workshop Pulsed RF Sources Linear Colliders,* Kanagawa, Japan, Apr. 8–12, 1996.

[8] ——, "The X-band klystron program at SLAC," in *Proc. 3rd Workshop Pulsed RF Sources Linear Colliders,* 1997, pp. 72–80.

[9] S. G. Tantawi *et al.*, "Compact X-band high-power load using magnetic stainless steel," in *Proc. Particle Accelerator Conf.* vol. 4, Dallas, TX, May 1–5, 1995, pp. 2132–2134.

Sami G. Tantawi (S'88–M'88) was born in Giza, Egypt, in 1962. He received the B.Sc. and M.Sc. degrees in electrical engineering from Cairo University, Giza, Egypt, in 1984 and 1987, respectively, and the Ph.D. degree in electrical engineering from the University of Maryland at College Park, in 1992.

Since 1992, he has been a Staff Physicist with the Stanford Linear Accelerator Center (SLAC), Stanford University, Stanford CA, and is currently the High-Power RF Group Leader. He is also with the Electrical Communications and Electronics Department, Cairo University, Giza, Egypt. His research interests includes vacuum electronics, high-power RF devices, modeling of RF structures, and planner RF circuits.

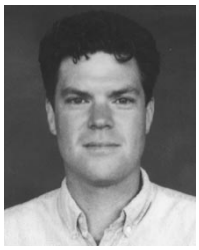

Roderick J. Loewen received the A.B. degree in physics from the University of California at Berkeley, in 1992, and is currently working toward the Ph.D. degree in physics at Stanford University, Stanford, CA. As a possible dissertation project, he anticipates helping the Stanford Linear Accelerator Center (SLAC) build the first small storage ring capable of producing a crystal electron beam.

He is a member of the Microwave Group, Stanford Linear Accelerator Center, Stanford University, Stanford, CA, where he develops technology for future electron linear accelerators. He pursues a wide interest of physics applications, including microwave cold-test techniques, RF simulation codes, low-emittance beams, and computer automation and control. He has written numerous test and measurement applications and holds a patent as a consultant in developing an automated control system used in medical accelerator manufacturing.

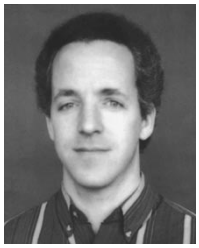

Christopher D. Nantista was born in New York, NY, in 1964. He received the B.A. degree in physics from Cornell University, Ithaca, NY, in 1986, and the M.S. and Ph.D. degrees in physics from the University of California at Los Angeles, in 1988 and 1994, respectively.

Since 1994, he has been with the Stanford Linear Accelerator Center, Stanford University, Stanford, CA, briefly in the Klystron and Microwave Department, and later in the Accelerator Theory and Special Projects Department. He has been chiefly involved in RF pulse compression experiments, beam instrumentation, and accelerator operations. He recently joined the High-Power Microwave Group, Accelerator Research Department A, where he concentrates on developing very high-power over-moded waveguide components for the RF distribution system of a next-generation linear collider. His research interests include the generation and manipulation of high-power microwaves, traveling-wave accelerator structures, beam physics, and accelerator applications.

Dr. Nantista is a member of Phi Beta Kappa and the American Physical Society.

Arnold E. Vlieks received the Ph.D. degree in physics from Ohio State University, Columbus, in 1973.

He has held post-doctoral positions at the University of Toronto, Toronto, Ont., Canada (1973–1976) CNRS, Orsay, France, (1976–1978), University of Zurich, Zurich, Switzerland (1978–1980), and the University of Muenster, Muenster, Germany (1980–1982). In 1982, he joined the Litton Electron Device Division, where he is involved with CCTWT's. He has been with the Stanford Linear Accelerator Center (SLAC), Stanford University, Stanford, CA, since 1985. During this time, he has been Group Leader of the Klystron R&D Group, NLC R&D Structures Group, and currently the High Power Test and Klystron Simulations Group. His current work deals with the simulation and high-power testing of Klystrons and low-loss RF components for the NLC, as well as high-power testing of high-gradient accelerator structures.